Impact of genetic dynamics and single-cell heterogeneity on development of nonstandard personalized medicine strategies for cancer

Robert A. Beckman[a,b,1], Gunter S. Schemmann[c,d], and Chen-Hsiang Yeang[a,e]

[a]Simons Center for Systems Biology, School of Natural Sciences, Institute for Advanced Study, Princeton, NJ 08540; [b]Center for Evolution and Cancer, Helen Diller Family Comprehensive Cancer Center, University of California, San Francisco, CA 94158; [c]Department of Molecular Biology, Princeton University, Princeton, NJ 08544; [d]World Water and Solar Technologies, Princeton, NJ 08540; and [e]Institute of Statistical Science, Academia Sinica, Taipei 115, Taiwan

Edited by Lawrence A. Loeb, University of Washington School of Medicine, Seattle, WA, and accepted by the Editorial Board July 13, 2012 (received for review February 29, 2012)

Cancers are heterogeneous and genetically unstable. Current practice of personalized medicine tailors therapy to heterogeneity between cancers of the same organ type. However, it does not yet systematically address heterogeneity at the single-cell level within a single individual's cancer or the dynamic nature of cancer due to genetic and epigenetic change as well as transient functional changes. We have developed a mathematical model of personalized cancer therapy incorporating genetic evolutionary dynamics and single-cell heterogeneity, and have examined simulated clinical outcomes. Analyses of an illustrative case and a virtual clinical trial of over 3 million evaluable "patients" demonstrate that augmented (and sometimes counterintuitive) nonstandard personalized medicine strategies may lead to superior patient outcomes compared with the current personalized medicine approach. Current personalized medicine matches therapy to a tumor molecular profile at diagnosis and at tumor relapse or progression, generally focusing on the average, static, and current properties of the sample. Nonstandard strategies also consider minor subclones, dynamics, and predicted future tumor states. Our methods allow systematic study and evaluation of nonstandard personalized medicine strategies. These findings may, in turn, suggest global adjustments and enhancements to translational oncology research paradigms.

systems biology | evolution | treatment strategy | targeted therapy | combinations

Current practice of personalized medicine designs therapy around stable differences between individual tumors. However, preexisting heterogeneity and genetic instability suggest the need for therapeutic strategies that address intratumoral heterogeneity and dynamics.

Genetic instability has been postulated to be central to tumor evolution (1). DNA sequencing reveals vast genetic variety associated with tumors: 20,000–30,000 mutations (2), about 1,000 of which are situated within exons (3) and 50–100 of which are nonsynonymous clonal mutations (4).

Mathematical models using the focused quantitative modeling methodology (5) have demonstrated that genetic instability enhances the efficiency of carcinogenesis, a result that is robust across all plausible parameter values and model types (5–7). More efficient mechanisms of carcinogenesis should be more common in clinical tumors. Driving the enhanced efficiency is the more rapid acquisition of oncogenic mutations, and quantitative analysis has suggested that tumors with three or fewer driver mutations might not be genetically unstable, a prediction that was recently confirmed for retinoblastoma (8). These models predicted heterogeneity within individual tumors, including spatial heterogeneity (9). Moreover, in contrast to an ordered series of mutational steps (10), the models predicted convergent and divergent evolution leading to overlapping but nonidentical sets of driver mutations within the same tumor (5–7). Recently, these predictions have been confirmed in renal cell cancer, where different mutations affecting the same pathway were spatially separated within the primary, reflecting convergent evolution (11). Pancreatic and breast cancers manifest genetic differences between the primary and metastases (12–15). Relapsed pediatric acute lymphoblastic leukemia (ALL) and primary adult ALL also reveal subclonal structure and divergent evolution (16–18). Additional diversity might, in principle, be detected by single-cell genomic analysis (19). In some cases, different driver mutations lead to different functional states, such as activation states of signaling pathways, within different parts of the tumor, as was seen for the mammalian target of rapamycin (*mTOR*) gene and associated pathway in renal cell cancer (11). Thus, intratumoral phenotypic and genotypic diversity is well established.

In the current personalized medicine paradigm, targeted therapies directed at specific molecular states replace nonspecific cytotoxics. Personalized medicine has the potential to transform cancer therapy and drug development (20). Tumors are stratified based on predictive biomarkers, which define molecular states, and are then matched to corresponding treatments.

A limitation is that the tumor is often characterized by a bulk measurement of the average molecular state, which may be dominated by the primary clone, without reflecting smaller subclones. A 1-cm^3 tumor mass will contain $\sim 10^9$ cells. Current sequencing technology can detect a sequence variation present in $\sim 1{:}10^4$ cells (19), meaning that in a 1-cm^3 tumor mass, a single variant cell is five orders of magnitude below the detection limit. Moreover, given the spatial heterogeneity demonstrated in renal cell cancer (11), even characterization of the dominant clone from a single location may be misleading (21).

Another concern is the frequent lack of biopsiable tumor throughout the clinical course, meaning that available tumor molecular information may not be current. Noninvasive methods, such as circulating tumor cells (22), plasma DNA (23), or functional imaging (24), could provide real-time information when sufficiently mature for general application. Imaging may potentially reveal spatial heterogeneity without multiple biopsies.

Dynamic resistance to therapy has been shown for many tumor types and by a variety of genetic and nongenetic mechanisms. In non-small cell lung cancer (NSCLC) treated with erlotinib

Author contributions: R.A.B., G.S.S., and C.-H.Y. designed research; R.A.B. and C.-H.Y. performed research; R.A.B., G.S.S., and C.-H.Y. contributed new reagents/analytic tools; R.A.B., G.S.S., and C.-H.Y. analyzed data; and R.A.B., G.S.S., and C.-H.Y. wrote the paper.

Conflict of interest statement: R.A.B. is a full-time employee of Daiichi Sankyo Pharmaceutical Development and is a stockholder in the Johnson & Johnson Corp. and in Daiichi Sankyo Pharmaceutical Development.

This article is a PNAS Direct Submission. L.A.L. is a guest editor invited by the Editorial Board.

[1]To whom correspondence should be addressed. E-mail: eniac1@snip.net.

This article contains supporting information online at www.pnas.org/lookup/suppl/doi:10.1073/pnas.1203559109/-/DCSupplemental.

or gefitinib, resistance mutations occur, most commonly in the target EGF receptor (EGFR) (22, 25). Other resistance mechanisms include activation of parallel signaling pathways, such as c-Met, through amplification, which is, at times, ligand-induced (26). Importantly, when erlotinib or gefitinib resistance develops, the drug's withdrawal may trigger tumor rebound, suggesting the persistence of a sensitive subpopulation below the detection limit (27). Resistance to crizotinib, a drug targeted to a unique fusion protein involving the anaplastic lymphoma kinase in NSCLC, has been documented due to mutations in the target, amplification of the target, loss of the original translocation leading to the fusion protein, increased signaling in the EGFR pathway (including 1 EGFR activating mutation), *c-Kit* amplification, and *KRAS* mutation, sometimes with more than one resistance mechanism in the same patient (28, 29). In chronic myelogenous leukemia, most therapeutic resistance is due to mutation in the targeted BCR-ABL fusion protein, and combinations may be important to delay the emergence of multiply resistant cells (30, 31). Nongenetic resistance mechanisms occur in tumors and may be immediate because they are wired into feedback loops in signaling pathways. Recent examples include resistance to vemurafenib in colorectal cancer cells (32, 33) and to PI3-kinase inhibitors (34) via up-regulation of upstream signaling pathways. Given these dynamics, there is a need to take possible future states into account, perhaps thinking several therapeutic maneuvers ahead.

We have developed methods for systematic evaluation of nonstandard personalized medicine strategies. A strategy is a data-driven method for planning a sequence of therapies, for example, when to give combination therapy as opposed to sequential high-dose therapies or when to change therapies. Like therapies, strategies may be individualized. Nonstandard personalized medicine strategies imply adjustments in current personalized medicine, as well as suggesting novel paradigms for oncology translational research.

Building on models of cancer therapy and resistance for chemotherapy (35, 36), we have created a mathematical model of cancer therapies, incorporating single-cell heterogeneity and (epi)genetic dynamics (all known mechanisms of genetic and epigenetic change) and examined the impact of various strategic choices on patient outcomes. We present an illustrative example and a clinical trial simulation with over 3 million virtual patients. We demonstrate that when subpopulations and genetic dynamics are taken into account, personalized medicine as currently practiced can be further improved by adopting new and sometimes counterintuitive strategies, including thinking several therapeutic moves ahead. The potential magnitude and significance of this improvement are substantial.

Results

Model. We created a mathematical model to predict patient outcomes (*Methods* and *SI Methods*). The model comprises two drugs, drug-1 and drug-2, and cell types representing four phenotypic states: sensitive to both drugs (S); resistant to drug-1, sensitive to drug-2 (R_1); resistant to drug-2, sensitive to drug-1 (R_2); and resistant to both drugs ($R_{1–2}$).

Tumors contain a continuously evolving mixture of the four cell types, each with its own characteristic exponential net growth rate. Cells transition between phenotypic states at each cell generation by heritable mechanisms. Each phenotypic state may correspond to many genotypes, and the net transition rate between phenotypic states is the sum of the rates from all possible mechanisms of genetic change affecting the sensitivity/resistance phenotype. Transient functional states, such as activation of signaling pathways, may be directly linked to genetic states, as recently demonstrated in renal cell cancer (11).

Assumptions include a dose-proportional decrease in the exponential growth constant with therapy. The total dose of both drugs in combination cannot exceed the normalized full dose of either drug, due to toxicity. The terms "drug-1" and "drug-2" may also refer to combinations directed at single states. For example, when there is hard-wired nongenetic resistance based on feedback activation of receptor tyrosine kinases (RTKs), such as occurs for vemurafenib and for PI3-kinase inhibitors (32–34), a combination that includes an inhibitor of the upstream RTK may be optimal for dealing with the underlying state. This optimized combination might be referred to as drug-1 because the core model deals only with genetic and epigenetic mechanisms of sensitivity and resistance (*SI Methods*).

The model outputs the number of cells of each type as a function of time and treatment. Patients begin with a minimally detectable 1-cm^3 lesion of 10^9 cells or a 5-cm^3 lesion and no $R_{1–2}$ cells. "Complete response" denotes a decrease in cells below 10^9. "Tumor progression" implies relapse and/or a doubling in cell number for detectable disease. "Relapse" denotes a return to $\geq 10^9$ cells. "Incurable" refers to any state containing $R_{1–2}$ cells. "Mortality" corresponds to a tumor burden of $\geq 10^{13}$ cells.

Illustrative Example. Fig. 1*A* illustrates how the model works for the current personalized medicine strategy. The patient presents with a single lesion of 10^9 S cells, as judged by next-generation sequencing, with sensitivity for variants of $1{:}10^4$ cells. Drug-1 is the best drug for S cells, causing a log kill within 23 d, whereas drug-2 slows S-cell growth by 90%. However, the case is constructed with undetected preexisting heterogeneity and dynamic asymmetry. Specifically, there are 10^4 preexisting R_1 cells, or 1 in 10^5, 10-fold below the level of detection. Second, transitions to drug-2 resistance occur at a rate of 4×10^{-7}, whereas acquisition of drug-1 resistance occurs 100 times more slowly (dynamic asymmetry). These assumptions are plausible for human cancers (37). In order for R_1 cells to outnumber R_2 cells, even though resistance to drug-2 occurs more quickly, a specific evolutionary history is required in which a recent event enhanced the ability to acquire drug-2 resistance. For example, if drug-2 resistance requires genetic change in both copies of a gene, change in one copy may have occurred, leading to the opportunity for rapid acquisition of drug-2 resistance through loss of heterozygosity.

In the current personalized medicine strategy (Fig. 1*A*), the patient is treated with drug-1, the best drug for S cells, based on the biopsy result and enjoys an initial complete response. However, 14 mo after initial diagnosis, relapse occurs and biopsy indicates pure R_1 cells (10^4 $R_{1–2}$ cells, resulting from random, passive acquisition of drug-2 resistance by the expanding R_1 clone, are undetected). Treatment with drug-2 ensues, resulting in another complete response. Twenty-eight months from initial diagnosis, the patient has an incurable relapse, predominantly with $R_{1–2}$ cells. The multiple relapses featured in this clinical course are typical in practice.

In contrast, in one possible nonstandard personalized medicine strategy (Fig. 1*B*), the physician considers the possible risk of undetected R_1 cells, and their ability to evolve rapidly into incurable $R_{1–2}$ cells. The physician may be considering genetic information about the likelihood of certain subclones available from the literature, such as the recent report of subclone frequencies in over 100 cases of triple-negative breast cancer (38). Accordingly, the patient is treated for 4 mo with the inferior drug for S cells, drug-2, allowing the tumor to grow slowly under careful observation but killing some of the R_1 cells if present. Subsequent switching to a 50:50 mix of the two drugs results in a complete response and an apparent cure.

By allowing the tumor to grow slowly rather than treating it with the better drug for the observed population, and by prioritizing rapid treatment of a hypothetical risk over optimally treating what is observed, the nonstandard personalized medicine approach has yielded a substantially improved outcome. Importantly, an upfront combination of the drugs might not have been sufficiently effective in preventing the emergence of the $R_{1–2}$ state.

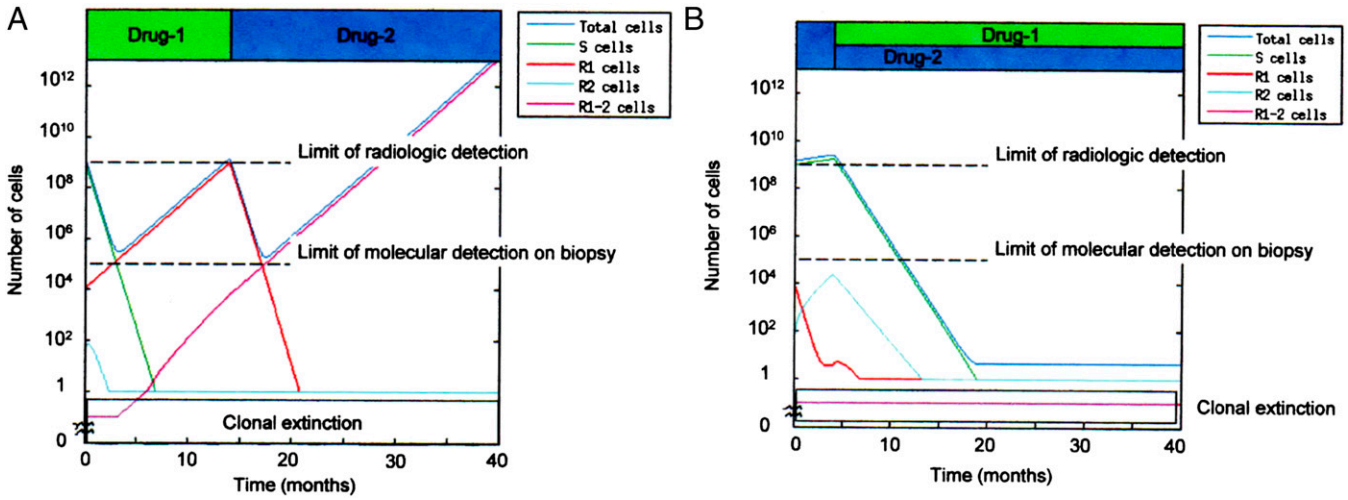

Fig. 1. Illustrative example contrasting current practice of personalized medicine (*A*) and nonstandard personalized medicine (*B*). Time (months) is on the *x* axis, and cell number is on the *y* axis. The total number of cells (*N*) is shown in blue (multiplied by 1.5 to create separation from the predominant population for clarity), S cells are shown in green, R_1 cells are shown in red, R_2 cells are shown in light blue, and R_{1-2} cells are shown in magenta. Treatments are indicated by the solid bars at the top: green is drug-1, blue is drug-2, and both colors indicate a combination. In the current personalized medicine strategy (*A*), the patient is treated with drug-1 and experiences a complete response, only to relapse 14 mo after diagnosis with R_1 cells. He/she is then treated with drug-2, experiencing a second complete response before he/she relapses with incurable R_{1-2} cells 28 mo after initial diagnosis. In the nonstandard personalized medicine strategy (*B*), the patient is treated with drug-2 for 4 mo to suppress a possible R_1 subpopulation even though it has not been detected. The bulk tumor slowly grows under observation. At 4 mo, treatment continues with an equal mixture of drug-1 and drug-2, resulting first in a complete response and then in an apparent cure. Note that initial treatment with an equal drug mixture would have been less effective in immediate eradication of R_1 cells, allowing more time for incurable R_{1-2} cells to evolve. Parameter values are provided in *SI Methods*.

Evolutionary dynamics and initial conditions affect the results. Thus, if the patient had an undetected subpopulation of R_2 cells rather than R_1 cells, the two sequences described above both lead to cure, the nonstandard sequence more rapidly (*SI Results* and Figs. S1 and S2).

A demonstration program for individual case analysis is provided on the Web (*SI Methods*).

Large-Scale Simulation. In the large-scale simulation (*Methods* and *SI Methods*), over 30 million parameter configurations are analyzed to assess the generality of the illustrative example, the potential benefits of nonstandard personalized medicine strategies, and the conditions under which minimizing the chance of transitions to incurability are an overriding strategic concern.

Parameters that were varied include proportions of different cell types, net growth rates, drug sensitivities, and transition rates between phenotypic states. Parameter ranges are derived from clinical, in vitro, and in vivo data sources, such as a series of 228 patients with pancreatic cancer with autopsies for 101 of them (39), and bracket all possible values to ensure inclusion of all possible biologically relevant scenarios. Within each parameter range, there are a large number of possible discrete values (e.g., many degrees of sensitivity/resistance are explored), and the simulation steps through every possible parameter combination once. Due to the inclusion of extreme parameter values, the parameter combinations were then prescreened, and the following were eliminated: (*i*) any combination in which one of the two drugs was not minimally effective against any cell type, because there are no strategic choices in this case, and (*ii*) any combination in which all treatment strategies resulted in survival greater than 4 y, corresponding to very slow growth rates or highly sensitive cells. Because the simulation was truncated at 5 y, it could not compare strategies in scenarios in which survival approached or exceeded this length of time (*SI Methods*).

Drug-1 is the better treatment against S cells. Survival is checked weekly, and treatments are adjusted every 45 d based on the various strategies. Ability to measure the cell populations is assumed. The simulation runs nearly 5 y (255 wk for economical data storage).

Six strategies are compared: current personalized medicine (strategy 0) and five alternatives (Table 1 and *SI Methods*). As in typical randomized oncology phase 3 trials, one strategy is "significantly better" than another if the superior strategy gives at least 8 wk of absolute improvement and 25% relative improvement in survival compared with the reference strategy. Strategy matters if at least one strategy is significantly better than another.

The resulting "clinical trial" contained 3,091,175 virtual patients, and strategy mattered for 1,001,868, showing a possible benefit of strategic choices. For the other 2 million patients, the current personalized medicine strategy gave results comparable to the other strategies. Moreover, the mean and median survival rates and percentage of 5-y survival rates seen for the simulated current personalized medicine strategy were similar to typical results for patients with metastatic solid tumors, confirming the ability of the simulation to give realistic results. Sampling of parameter values in the simulation may or may not reflect their unknown distribution in patients.

The current personalized medicine strategy was generally inferior. Other strategies produced double the mean and median survival rates (Table 2). The Kaplan–Meier survival plot over evaluable virtual patients (Fig. 2) shows a dramatic benefit of nonstandard strategies over current personalized medicine. Five-year survivorship is 0.7% for current personalized medicine and 17–20% for the other strategies (Table 2). Strategy 2.2, similar to the illustrative example, is most frequently significantly superior to the other strategies (Table 2). No strategy is inferior to the current personalized medicine strategy as frequently as it is superior, nor is the current personalized medicine strategy ever the best (Table 2).

We examined what features are required for strategy to matter (*SI Results*). Either preexisting heterogeneity or rapid genetic dynamics are generally required for strategy to matter. Given no R_1 preexisting (with drug-1 as the better drug for S, only R_1 creates strategic dilemmas), and low $S \rightarrow R_1$ transition rates,

Table 1. Treatment strategies

Strategy	Summary	Details
0	Current personalized medicine paradigm	The patient is treated with the best drug for the observed predominant cell type and switched to the alternative drug on tumor progression or relapse
1	Minimize total cell population (i.e., give the drug combination that the model predicts will do so)	Minimized at next 45-day time point
2.1	Minimize the chance of developing incurable R_{1-2} cells unless there is radiologically detectable disease burden above a "threshold" cell number; then, minimize total population	Threshold cell number to be considered radiologically detectable is 10^9 or more; minimization applies to next 45-day time point
2.2	Minimize the chance of developing incurable R_{1-2} cells unless there is a large disease burden above a threshold cell number; then, minimize total population	Threshold cell number to be considered large disease burden is 10^{11} or more; minimization applies to next 45-day time point
3	Minimize the total population unless there is an immediate threat of developing an incurable R_{1-2} cell; then, minimize R_{1-2} cells	Immediate threat is defined as predicted number of R_{1-2} cells ≥ 1 at next 45-day time point
4	Treat the most proximal threat	Estimated time to mortality from each cell type is compared with estimated time to the first incurable R_{1-2} cell; the threat estimated to have the shortest time is prioritized in treatment; mortality is defined as a tumor cell burden of 10^{13}

A strategy is a data-driven method for planning a sequence of therapies, based on both individual patient data and general oncology knowledge. The strategies discussed in this paper are examples only and are not meant to be a comprehensive list.

strategy mattered in 1.1% of evaluable cases, compared with 32.4% of evaluable cases in the overall simulation. However, we do not need both preexisting heterogeneity and rapid genetic dynamics for strategy to matter: the number of cases where it matters is relatively constant as either of these parameters alone is varied. Finally, asymmetry of transition rates, sensitivity patterns, or preexisting subpopulations are not required, not occurring more often than expected in cases where strategy matters. These results suggest that the illustrative example represents only one of many scenarios where strategy matters.

Strategy 1 differs from strategies 2–4 in that it never prioritizes prevention of R_{1-2} cell formation; instead, it simply minimizes the predicted total population. In most cases, the full benefit can be captured with this simple approach alone. By estimating the time to either incurability (τ_{1-2}) or death due to other populations, one can determine if τ_{1-2} is the shorter, indicating that the threat of incurability is more imminent than the threat of mortality from all other subpopulations (*SI Methods*). Strategy 1 is more likely to be inferior to strategies 2–4 if this condition is met (Table S1).

Discussion

We have shown that genetic dynamics and single-cell heterogeneity can have a significant impact on optimal personalized medicine strategies and that striking therapeutic gains are possible. The magnitude of the average benefit would have been significant even if applicable only to a single class of therapies and a restricted subset of patients. In contrast, a comprehensive exploration of oncology parameter space via simulation indicates that the benefit is applicable across a very broad range of therapy and tumor characteristics. We believe the systematic study of nonstandard personalized medicine strategies is an important area for experimental and theoretical investigation.

The current study is a proof of concept using a simple, focused model and is not intended to represent all known complexities of tumor behavior at either the single-cell level or the population level, where complex ecologies may provide further selection for heterogeneity. With appropriate sensitivity analyses, simple models can answer high-level focused questions ("Is the current strategy for personalized therapy of cancer the best possible?") in a way that is clear and valid across a broad range of cases (5). In this paper, we have asked this high-level focused question and tested its generality over millions of possible scenarios, with comprehensive parameter ranges based on clinical and experimental data. The high-level conclusions are shown to be robust. However, detailed conclusions will vary, depending on more detailed tumor behavior, and the model must be customized for each tumor type under consideration based on molecular and empirical knowledge. In *SI Methods*, we discuss a framework for linking the simple core strategy model presented here to molecular and

Table 2. Comparison of treatment strategy results

Strategy	0	1	2.1	2.2	3	4
Median survival*,wk	26	58	58	58	58	51
Mean survival*, wk	48.4	95.3	95.7	96.5	96.8	91.7
Survival at 5 y, %	0.7	18.7	19.0	19.7	19.4	17.6
No. of cases strategy numerically better than all others	1,538	244	4,292	60,599	2,124	2,206
No. of cases strategy significantly† better than all others	0	0	24	2,367	157	315
No. of cases significantly† better than strategy 0	N.A.	951,165	947,634	947,568	971,111	823,939
No. of cases significantly† worse than strategy 0	N.A.	6,808	5,725	2,762	630	27,597

Strategy results are based on performance in a virtual clinical trial of over 3 million evaluable cases. Evaluable means that both drugs met minimal criteria for efficacy, providing strategic choices, and that the minimum survival of the worst strategy is ≤80% of the simulation length, allowing room for other strategies to demonstrate superiority. Strategies are defined in Table 1. N.A., not applicable.
*Simulation truncated at 255 wk, which is nearly 5 y, and data can be stored as 8 bits.
†Significantly better means at least 8 wk of absolute improvement and 25% relative improvement compared with the reference strategy, in analogy to the typical minimum improvement deemed clinically significant in randomized phase 3 trials in cancer.

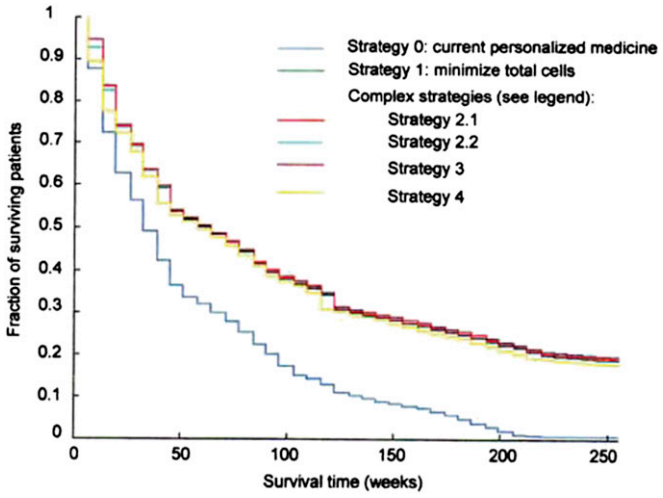

Fig. 2. Kaplan–Meier survival curves of a virtual clinical trial incorporating different strategies. Approximately 3 million evaluable virtual patients were treated with each of the strategies. The *x* axis shows time (weeks), and the *y* axis shows the surviving patient fraction. Strategy 0 (dark blue) is the current personalized medicine strategy: treatment with the best drug for the observed predominant cell type and switching to the alternative drug on tumor progression or relapse. Strategy 1 (green) minimizes total cell numbers at the next time point. Strategy 2.1 (red) minimizes the chance of developing incurable R_{1-2} cells at the next time point unless the patient has detectable disease (10^9 cells); at that point, total cell number is minimized. Strategy 2.2 (light blue) minimizes the chance of developing incurable R_{1-2} cells at the next time point unless the patient has a high disease burden (10^{11} cells); at that point, the total number of cells is minimized. Strategy 3 (magenta) minimizes the total cells at the next time point unless the predicted R_{1-2} cell population at that time point is ≥ 1; in that case, the R_{1-2} cell population is minimized. Strategy 4 (olive) predicts the time to mortality from each cell population and the time to "incurability" from forming R_{1-2} cells, prioritizing treatment of the most imminent threat at the next time point.

empirical knowledge of specific tumors and therapies, including complications not represented in the core model.

States in the core model correspond to heritable drug sensitivity/resistance phenotypes over all available drugs, and there may be a very large number of underlying molecular states that contribute to a single phenotype. The condensation from a large number of molecular/genetic states to a smaller number of clusters of phenotypic sensitivity/resistance profiles is essential to allow computationally feasible examination of highly innovative strategies, especially when real systems with more than two therapies are considered. Intermediate sensitivity states that may arise from haploinsufficiency or gene dosage effects must also be considered in a full model.

Similarly, the transition rate from phenotype A to phenotype B is actually the sum of individual rates from all known genetic and epigenetic mechanisms of transition at all relevant loci. Recent work on mechanisms of resistance to crizotinib (28, 29) gives an example of how multiple mechanisms can contribute to the resistance phenotype, and these processes would all have to be identified, and rates summed, to give a net transition rate. Nongenetic resistance mechanisms are addressed separately (*SI Methods*).

Relevant data sources for condensing molecular states into shared sensitivity phenotypes, or for summing transition rates to get a net transition rate, include molecularly annotated cell line panels (40), genetic data at the subclonal level from large cohorts of patients (38), computational integration of data from multiple sources along curated signaling pathways (41), and high-throughput functional genomic screens using siRNA and shRNA (42).

This illustrates the principle of linked models, some relatively simple, feeding each other information to represent a complex system. The information about the tumor type and therapies of interest can be calculated once and used to inform the focused core model through its impact on the probability distributions of parameter values. In a separate step, the core model would calculate the patient outcome resulting from a series of innovative treatment strategies.

In a comprehensive model, some information will be uncertain or missing. Therefore, advanced techniques for optimizing strategies in the face of uncertainty will be required (43). It is unknown how much missing information can be tolerated without affecting the utility of the models. This is an important area for future research. The models are a supplement to, rather than a substitute for, sound clinical judgement.

Because the number of phenotypic states is much smaller than the number of molecular states, a strategic model for cancer therapy could also become an organizing principle for our ever-expanding body of molecular data and understanding. Areas needed for progress in the treatment strategy model may correspond to key research and drug discovery priorities.

We have introduced methodology for systematic study of nonstandard personalized medicine strategies. There are key differences from the current personalized medicine paradigm. Instead of focusing on majority populations at diagnosis or at the treatment time, nonstandard personalized medicine strategies consider all subpopulations and the whole time course of possible states. In particular, nonstandard personalized medicine strategies may emphasize preventing fully resistant or incurable states by attacking their immediate precursors (*SI Methods*, Fig. S3, and Table S2). This leads to the possibility that, assuming sufficient knowledge, one might not treat initially with the targeted agent that is most effective against the predominant observed population. Although we may not have sufficient knowledge to adopt such a counterintuitive strategy at the moment, our molecular knowledge of cancer, its therapy, and its evolution is increasing rapidly. In the future, initial treatment might consider the probability distribution of current states below the detection limit and even future states. We note that current combination chemotherapy already incorporates some of these principles, although nonstandard personalized medicine may not always recommend combinations.

To facilitate application of nonstandard personalized medicine strategies, current efforts in translational oncology should be augmented in specific ways. This, in turn, may provide new directions for these fields.

Currently, biological samples exist predominantly from diagnosis and less frequently from relapse. In contrast, we suggest working backward from the fatal end states. This would require advance directives from healthy individuals to donate tumor tissue immediately on death due to cancer in much the same way that we all specify, when healthy, that we will donate organs, when feasible, after accidental death. Cell lines, patient sample banks, and patient-derived xenografts should be established from these sources, ideally paired with diagnostic samples and treatment course information.

Experimental validation of this approach could involve an in vitro or in vivo system determined by sensitivity and resistance to two drugs, with known underlying heritable molecular types. Predictable and sufficient transition rates are required. Cell populations and survival rates need to be determined under different strategic paradigms with varying initial subpopulations.

Application of nonstandard personalized medicine to cancer requires experimental validation, detailed integration of current knowledge into customized models, and further conceptual and technological advances. However, we have shown that the benefit of such an approach, when successfully applied, will be highly significant.

Methods

Model. Denote a four-component vector, $\vec{x} = (x_S, x_{R1}, x_{R2}, x_{R1-2})$, as the cell population of each class. We assume that cell death rates are zero in the absence of therapy, that all cells have the same growth rate, and that the drugs work by increasing cell death. For each class, $i \in \{S, R_1, R_2, R_{1-2}\}$, the net growth rate is $g_0 x_i + \sum_{j \neq i} T(i,j) g_0 x_j - (S_a(i,1) d_1 + S_a(i,2) d_2) x_i$. The first term corresponds to the growth rate of cell type i with a rate g_0 shared by all cell types. The second term corresponds to the transitions from all other cell types, where $T(i,j)$ specifies the transition rate (per cell per generation) from cell type j to i. We assume that (*i*) transition rates from resistant to sensitive cell types are negligible, (*ii*) the transition rate of acquiring the resistance to one drug is independent of the resistance phenotype to another drug, and (*iii*) transition rates of acquiring double resistance in one step are negligible. Thus, $T(R_1, S) = T(R_{1-2}, R_2)$, $T(R_2, S) = T(R_{1-2}, R_1)$, and all other entries of T are zero. The third term corresponds to the treatment-caused cell death, where $(d_1, d_2)^T \equiv \vec{d}$ represents the normalized dosages of the two drugs (d_1 is drug-1 and d_2 is drug-2) with the constraints $0 \leq d_1, d_2, d_1 + d_2 \leq 1$ and $S_a(i,1), S_a(i,2)$ represents the sensitivities of cell type i to drug-1 and drug-2. The population dynamics of the four cell types can be compactly expressed as a matrix differential equation:

$$\frac{d\vec{x}}{dt} = \left[(I+T) g_0 - diag\left(S_a \vec{d}\right) \right] U(\vec{x} - 1) \vec{x}, \qquad [1]$$

where I denotes a four-by-four identity matrix and $diag(.)$ denotes an operator of placing vector components on the diagonal entries of a zero matrix. $U(\vec{x} - 1)\vec{x}$ sets component values to 0 if they are less than 1; that is, $U(\vec{x} - 1) = 0$ for $x < 1$ and $U(\vec{x} - 1) = 1$ for $x \geq 1$. This term stipulates that fractional cell numbers (less than 1 cell) do not contribute to cell division.

This equation was implemented in MATLAB 7.7.0 (R2008b; MathWorks) and manually explored on a Gateway T-6836 computer with the Windows Vista (Microsoft Corporation) operating system and a 2.0-GHz Intel Core 2 Duo CPU T5750 processor to produce the illustrative example.

Large-Scale Simulation. A large-scale simulation was carried out to compare a current personalized medicine strategy with five alternative strategies for over 30 million configurations of nine parameters involving initial populations of each cell type, growth rates, drug sensitivities, and transition rates. Detailed definitions of the strategies and the parameters, as well as ranges and values of the parameters, are provided in *SI Methods*.

We can solve Eq. **1** analytically given a time-varying dosage $\vec{d}(t)$ and the initial population $\vec{x}(0)$. Insert "break points" in the time interval whenever $\vec{d}(t)$ changes or a component in $\vec{x}(t)$ crosses 1 (increases from a fractional number to a number larger than 1 or vice versa). Between any two consecutive break points, the term on the right-hand side of Eq. **1**, $[(I+T)g_0 - diag(S_a\vec{d})]U(\vec{x} - 1) \equiv A$, is a constant matrix. The solution of a first-order linear matrix differential equation $\frac{d\vec{x}(t)}{dt} = A\vec{x}(t)$ is $\vec{x}(t) = e^{At}\vec{x}(0)$. Hence, $\vec{x}(t)$ can be obtained by solving the first-order linear matrix differential equation piecewise.

We implemented the simulation in a C program and ran it on 23 Hewlett Packard DL360 G7 servers in parallel. Each server contains dual Intel(R) Xeon (R) CPUs E5520 with 2.27GHz and 24 GB of main memory. The running time was approximately 1 day.

ACKNOWLEDGMENTS. We thank Arnold Levine, Director of the Simons Center for Systems Biology, Institute for Advanced Study, and Peter Goddard, Director of the Institute for Advanced Study, for hosting R.A.B. and C.H.Y. at the inception of this work. We thank Ming-Ren Yen for assistance with the large-scale simulation and Robert Shin-sheng Yuan and Cin-di Wang for Web site programming and design. We also thank Prashanth Ak, Alessandra Cesano, Robert Corringham, Lawrence Loeb, Eric Maskin, Frank McCormick, Paul Meltzer, Daniel Notterman, David Parkinson, Daniel Rabin, Guna Rajagopal, Hatem Sabaawy, Richard Simon, Alexei Vazquez, Daniel von Hoff, and Susan J. Ward for helpful discussions.

1. Loeb LA, Springgate CF, Battula N (1974) Errors in DNA replication as a basis of malignant changes. *Cancer Res* 34:2311–2321.
2. Pleasance ED, et al. (2010) A comprehensive catalogue of somatic mutations from a human cancer genome. *Nature* 463:191–196.
3. Wood LD, et al. (2007) The genomic landscapes of human breast and colorectal cancers. *Science* 318:1108–1113.
4. Parsons DW, et al. (2008) An integrated genomic analysis of human glioblastoma multiforme. *Science* 321:1807–1812.
5. Beckman RA (2010) Efficiency of carcinogenesis: Is the mutator phenotype inevitable? *Semin Cancer Biol* 20:340–352.
6. Beckman RA, Loeb LA (2006) Efficiency of carcinogenesis with and without a mutator mutation. *Proc Natl Acad Sci USA* 103:14140–14145.
7. Beckman RA (2009) Mutator mutations enhance tumorigenic efficiency across fitness landscapes. *PLoS ONE* 4:e5860.
8. Zhang J, et al. (2012) A novel retinoblastoma therapy from genomic and epigenetic analyses. *Nature* 481:329–334.
9. Loeb LA, Bielas JH, Beckman RA (2008) Cancers exhibit a mutator phenotype: Clinical implications. *Cancer Res* 68:3551–3557, discussion 3557.
10. Fearon ER, Vogelstein B (1990) A genetic model for colorectal tumorigenesis. *Cell* 61: 759–767.
11. Gerlinger M, et al. (2012) Intratumor heterogeneity and branched evolution revealed by multiregion sequencing. *N Engl J Med* 366:883–892.
12. Yachida S, et al. (2010) Distant metastasis occurs late during the genetic evolution of pancreatic cancer. *Nature* 467:1114–1117.
13. Klein CA, Hölzel D (2006) Systemic cancer progression and tumor dormancy: Mathematical models meet single cell genomics. *Cell Cycle* 5:1788–1798.
14. Fujii H, Marsh C, Cairns P, Sidransky D, Gabrielson E (1996) Genetic divergence in the clonal evolution of breast cancer. *Cancer Res* 56:1493–1497.
15. Shah SP, et al. (2009) Mutational evolution in a lobular breast tumour profiled at single nucleotide resolution. *Nature* 461:809–813.
16. Mullighan CG, et al. (2008) Genomic analysis of the clonal origins of relapsed acute lymphoblastic leukemia. *Science* 322:1377–1380.
17. Anderson K, et al. (2011) Genetic variegation of clonal architecture and propagating cells in leukaemia. *Nature* 469:356–361.
18. Notta F, et al. (2011) Evolution of human BCR-ABL1 lymphoblastic leukaemia-initiating cells. *Nature* 469:362–367.
19. Fox EJ, Salk JJ, Loeb LA (2009) Cancer genome sequencing—An interim analysis. *Cancer Res* 69:4948–4950.
20. Beckman RA, Clark J, Chen C (2011) Integrating predictive biomarkers and classifiers into oncology clinical development programmes. *Nat Rev Drug Discov* 10:735–748.
21. Longo DL (2012) Tumor heterogeneity and personalized medicine. *N Engl J Med* 366: 956–957.
22. Maheswaran S, et al. (2008) Detection of mutations in EGFR in circulating lung-cancer cells. *N Engl J Med* 359:366–377.
23. Wang S, et al. (2010) Potential clinical significance of a plasma-based KRAS mutation analysis in patients with advanced non-small cell lung cancer. *Clin Cancer Res* 16: 1324–1330.
24. Orlova A, et al. (2007) Synthetic affibody molecules: A novel class of affinity ligands for molecular imaging of HER2-expressing malignant tumors. *Cancer Res* 67:2178–2186.
25. Kobayashi S, et al. (2005) *EGFR* mutation and resistance of non-small-cell lung cancer to gefitinib. *N Engl J Med* 352:786–792.
26. Turke AB, et al. (2010) Preexistence and clonal selection of MET amplification in EGFR mutant NSCLC. *Cancer Cell* 17(1):77–88.
27. Riely GJ, et al. (2007) Prospective assessment of discontinuation and reinitiation of erlotinib or gefitinib in patients with acquired resistance to erlotinib or gefitinib followed by the addition of everolimus. *Clin Cancer Res* 13:5150–5155.
28. Lovly CM, Pao W (2012) Escaping ALK inhibition: Mechanisms of and strategies to overcome resistance. *Sci Transl Med* 4:120ps2.
29. Katayama R, et al. (2012) Mechanisms of acquired crizotinib resistance in ALK-rearranged lung cancers. *Sci Transl Med* 4:120ra17.
30. Bradeen HA, et al. (2006) Comparison of imatinib mesylate, dasatinib (BMS-354825), and nilotinib (AMN107) in an *N*-ethyl-*N*-nitrosourea (ENU)-based mutagenesis screen: High efficacy of drug combinations. *Blood* 108:2332–2338.
31. Shah NP, et al. (2007) Sequential ABL kinase inhibitor therapy selects for compound drug-resistant BCR-ABL mutations with altered oncogenic potency. *J Clin Invest* 117: 2562–2569.
32. Prahallad A, et al. (2012) Unresponsiveness of colon cancer to BRAF(V600E) inhibition through feedback activation of EGFR. *Nature* 483:100–103.
33. Solit DB, Jänne PA (2012) Translational medicine: Primed for resistance. *Nature* 483: 44–45.
34. Chandarlapaty S, et al. (2011) AKT inhibition relieves feedback suppression of receptor tyrosine kinase expression and activity. *Cancer Cell* 19(1):58–71.
35. Goldie JH, Coldman AJ (1979) A mathematic model for relating the drug sensitivity of tumors to their spontaneous mutation rate. *Cancer Treat Rep* 63:1727–1733.
36. Norton L, Simon R (1976) Tumor size, sensitivity to therapy and the design of treatment protocols. *Cancer Treat Rep* 61:1307–1317.
37. Beckman RA, Loeb LA (2005) Negative clonal selection in tumor evolution. *Genetics* 171:2123–2131.
38. Shah SP, et al. (2012) The clonal and mutational evolution spectrum of primary triple-negative breast cancers. *Nature* 486:395–399.
39. Haeno H, et al. (2012) Computational modeling of pancreatic cancer reveals kinetics of metastasis suggesting optimum treatment strategies. *Cell* 148:362–375.
40. Barretina J, et al. (2012) The Cancer Cell Line Encyclopedia enables predictive modelling of anticancer drug sensitivity. *Nature* 483:603–607.
41. Heiser LM, et al. (2012) Subtype and pathway specific responses to anticancer compounds in breast cancer. *Proc Natl Acad Sci USA* 109:2724–2729.
42. Jiang H, Pritchard JR, Williams RT, Lauffenburger DA, Hemann MT (2011) A mammalian functional-genetic approach to characterizing cancer therapeutics. *Nat Chem Biol* 7(2):92–100.
43. Dutta PK (2005) *Strategies and Games: Theory and Practice* (MIT Press, Cambridge, MA).

Supporting Information

Beckman et al. 10.1073/pnas.1203559109

SI Results

Analysis of Case Related to the Illustrative Example. The outcomes and optimal strategy depend heavily on the initial conditions. In the illustrative example given the in main text, in which there is an undetected population of cells resistant to drug-1 and sensitive to drug-2 [R_1, which is the best drug for cells sensitive to both drugs (S)], a strategy that considers the risk of undetected R_1 by treating with drug-2 for 4 mo followed by an equal combination of drug-1 and drug-2 is superior to the current personalized medicine strategy, resulting in cure, whereas the current personalized medicine strategy results in incurable relapse at 28 mo.

If, on the other hand, we consider slightly different initial conditions, where the patient begins with 10^9 S cells and 10^4 cells resistant to drug-2 and sensitive to drug-1 (R_2), there is no obvious dilemma, because drug-1 is the best drug for both. We compared the conventional personalized medicine strategy (Fig. S1) with a nonstandard strategy in which we treat with drug-1 for 4 mo, followed by an equal combination of both drugs (Fig. S2).

In the conventional personalized medicine strategy, we treat with drug-1, and the patient first responds and then relapses with the R_1 cell type, which was not preexisting but arose from S cells by mutation. Subsequent treatment with drug-2 cures the patient at 32 mo.

In the nonstandard personalized medicine strategy, the patient is cured in 10 mo without enduring relapse, because the combination prevents relapse with R_1 cells.

By the criteria of our main analysis, the strategies would be considered equal, because both result in cure and long-term survival; however, even in this case, a nonstandard strategy is better in that the patient is cured more quickly and does not suffer a relapse before cure. Moreover, if the simulation were stochastic rather than deterministic, one would likely see a greater risk for not being cured with the conventional personalized medicine strategy.

When Does Strategy Matter? The illustrative case in the main text had three main features: preexisting heterogeneity below the level of detection, with the minority subpopulation resistant to the recommended drug for the main population; rapid genetic dynamics; and asymmetry (unequal transition rates to resistance to the two different drugs, which could also manifest as different degrees of resistance to the two drugs or as unequal amounts of the possible resistant subpopulations). We examined the ~3 million evaluable virtual cases in the simulation, for ~1 million of which "strategy mattered," to see if the features of the illustrative case were required for strategy to matter. "Strategy matters" was defined as at least one strategy significantly superior to another, meaning at least 8 wk of absolute improvement and 25% relative survival advantage of the superior strategy over the inferior reference strategy.

In the simulation, d_1 was the superior drug by convention, meaning that R_1 could be a minority subpopulation resistant to the "better drug." If we look at the cases for the seven values of x_{R1}/N ($N = x_S + x_{R1} + x_{R2} + x_{R1-2}$) allowed in the simulation, where R_{1-2} are cells resistant to both drug-1 and drug-2, we see there is not a dramatic dependence of the number of cases where strategy matters on preexisting heterogeneity alone. In fact, there are numerous cases where strategy matters where there is no preexisting heterogeneity.

$x_{R1}/N = 0$; 81,624 cases
$x_{R1}/N = 1 \times 10^{-9}$; 152,246 cases
$x_{R1}/N = 1 \times 10^{-7}$; 170,268 cases
$x_{R1}/N = 1 \times 10^{-5}$; 165,043 cases
$x_{R1}/N = 1 \times 10^{-3}$; 176,931 cases
$x_{R1}/N = 1 \times 10^{-1}$; 158,660 cases
$x_{R1}/N = 9 \times 10^{-1}$ (no longer the minority population); 97,096 cases

In a similar manner, we looked to see if there is a dependence, in the 1 million cases where strategy mattered, on the rate of transition to resistance to either d_1 or d_2. Again, there was no dramatic dependence of the number of cases where strategy mattered on either of these single parameters.

$S \rightarrow R_1$ transition rate $= 1 \times 10^{-11}$; 154,564 cases
$S \rightarrow R_1$ transition rate $= 2.154 \times 10^{-10}$; 154,221 cases
$S \rightarrow R_1$ transition rate $= 4.642 \times 10^{-9}$; 154,288 cases
$S \rightarrow R_1$ transition rate $= 1 \times 10^{-7}$; 150,576 cases
$S \rightarrow R_1$ transition rate $= 2.154 \times 10^{-6}$; 141,533 cases
$S \rightarrow R_1$ transition rate $= 4.642 \times 10^{-5}$; 130,626 cases
$S \rightarrow R_1$ transition rate $= 1 \times 10^{-3}$; 116,060 cases
$S \rightarrow R_2$ transition rate $= 1 \times 10^{-11}$; 144,627 cases
$S \rightarrow R_2$ transition rate $= 2.154 \times 10^{-10}$; 162,919 cases
$S \rightarrow R_2$ transition rate $= 4.642 \times 10^{-9}$; 161,834 cases
$S \rightarrow R_2$ transition rate $= 1 \times 10^{-7}$; 148,738 cases
$S \rightarrow R_2$ transition rate $= 2.154 \times 10^{-6}$; 143,135 cases
$S \rightarrow R_2$ transition rate $= 4.642 \times 10^{-5}$; 130,219 cases
$S \rightarrow R_2$ transition rate $= 1 \times 10^{-3}$; 110,396 cases

To investigate the importance of asymmetry, we compared the number of expected vs. observed symmetrical cases, where $R_1 = R_2$, relative resistance of R_1 to d_1 = relative resistance of R_2 to d_2, and transition rate to resistance to d_1 = transition rate to resistance to d_2. If there are fewer numbers of symmetrical cases where strategy matters than expected based on their possibility of being chosen (generally 1/7-fold the number of cases, except for the subpopulation numbers where their sum cannot exceed N), this would imply a tendency to asymmetry. There was no marked tendency to asymmetry based on number of symmetrical cases where strategy matters being similar to that expected:

Equal numbers of two minority subpopulations: 143,124 cases expected and 137,614 cases observed
Equal relative resistance to two drugs: 166,978 cases expected, and 161,244 cases observed
Equal transition rates to resistance to two drugs: 166,978 cases expected and 139,523 cases observed

Finally, we asked whether strategy could still matter in the absence of both preexisting heterogeneity and rapid genetic dynamics. The data suggest that for strategy to matter, at least one of those two elements should usually be present. The expected number of cases where strategy matters and where there are no preexisting R_1 cells and the lowest transition rate to R_1 cells is $1/7^2$-fold the number of cases where strategy matters, or 20,466 cases. In contrast, only 659 such cases are observed. Moreover, ~85% of these cases occur in a narrow band of growth rates from 1.8 to 5×10^{-5}. Whereas strategy matters in 32.4% of cases in the simulation, in the absence of both preexisting heterogeneity and rapid genetic dynamics, strategy matters in only 1.1% of the cases.

Overall, the results suggest that the conditions of the illustrative example are only one of many possible situations where strategy might matter. Preexisting heterogeneity or genetic instability may be required for cases where strategy matters to be frequent.

SI Methods

Cancer Model. The model can be compactly expressed as a matrix differential equation:

$$\frac{d\vec{x}}{dt} = \left[(I+T)g_0 - diag\left(S_a\vec{d}\right)\right]U\left(\vec{x}-1\right)\vec{x}, \qquad \textbf{[S1]}$$

where I denotes a four-by-four identity matrix and $diag(.)$ is an operator of placing vector components on the diagonal entries of a zero matrix. T is a four-by-four transition rate matrix, and S_a is a four-by-two matrix of drug sensitivities. $U(\vec{x}-1)\vec{x}$ is the Heaviside step function that sets component values to 0 if they are less than 1, that is, $U(x-1)=0$ for $x<1$ and $U(x-1)=1$ for all $x \geq 1$. This term stipulates that fractional cell numbers (less than 1 cell) do not contribute to cell division.

Demonstration Program for Calculating Individual Cases (Web Site). We have provided a demonstration program for calculating individual cases. To try it, click on the URL (http://cancermodel.stat2.sinica.edu.tw/cell_n_drug). Contact the authors with questions or comments.

Comparison of Current Personalized Medicine Strategy with Nonstandard Personalized Medicine Strategies. We have introduced methodology for systematic study of next-generation personalized medicine strategies. Key differences from the current personalized medicine paradigm are summarized in Table S2. Instead of focusing on majority populations at diagnosis or at the time of treatment (initial or current predominant states), next-generation personalized medicine strategies consider all subpopulations and the whole time course of possible states. In particular, next-generation personalized medicine strategies may emphasize preventing fully resistant or incurable end states by attacking their immediate precursors, the penultimate treatable states (Fig. S3). This leads to the possibility that, assuming sufficient knowledge, one might not treat initially with the targeted agent that is most effective against the predominant observed population. Although we may not have sufficient knowledge to adopt such a counterintuitive strategy at the moment, our molecular knowledge of cancer, its therapy, and its evolution is increasing rapidly. In the future, initial treatment might consider the probability distribution of current states below the detection limit and even future states.

Treatment Strategies. Our objective is to demonstrate the advantages of strategy-based treatments (adjusting drug dosages according to the predicted risks) over the current paradigm of personalized medicine (choosing treatments based on the molecular properties of the predominant subpopulation and changing drugs when tumor progression or relapse is detected). We note that more complex individualized strategies, such as the ones below, are also personalized medicine, just not as currently practiced. To fulfill this goal, we implemented six treatment strategies in simulation studies. We assume in this simulation that the cell type S is more sensitive to drug-1 (d_1) than to drug-2 (d_2) and that the cell type R_2 is more sensitive to d_1 than the cell type R_1 is to d_2. Hence, d_1 is overall the superior drug.

Strategy 0: Current personalized medicine strategy. Initially, treat the patient with d_1 alone if $\frac{x_{R1}}{x_S+x_{R1}+x_{R2}+x_{R1-2}} \leq 0.5$ (i.e., the R_1 population does not dominate the tumor). Otherwise, treat the patient with d_2 alone. A nadir is a local minimum of the total population among the time-series profile where the current treatment is maintained. Maintain the current treatment until either one of the following events occurs: (*i*) The total population reaches twice the nadir population [Response Evaluation Criteria In Solid Tumors (RECIST) tumor progression scaled up to represent tumor volume rather than a single linear dimension], or (*ii*) the total population reemerges from a level below the detection threshold (10^9; relapse). If either (*i*) or (*ii*) occurs, switch to another drug. Strategy 0 mimics the current paradigm of personalized medicine in that the initial treatment is selected by molecular characterization of the predominant population and classification into one of the four cell types.

Strategy 1: Minimize the predicted total population. Every 45 days, adjust $\vec{d}(t)$ to minimize the predicted total population by maintaining the (hypothetical) treatment over a period of "lookahead time." Vary d_1 and d_2 between 0 and 1 with a 0.01 interval. For each dosage combination, evaluate the predicted total population by solving Eq. **S1**, with the initial populations being the currently observed populations of each cell type, $\vec{d}(t)$ being fixed to the given dosage combination, and the duration being the lookahead time (45 days). Choose the dosage combination that minimizes the predicted total population.

Strategy 2: Minimize the risk of incurable cells developing unless there is an immediate threat of mortality. Every 45 days, adjust $\vec{d}(t)$ to minimize the predicted R_{1-2} population if the total population does not exceed a threshold. R_{1-2} is resistant to both drugs; therefore, it is often incurable. All simulations start with an R_{1-2} population of 0. By preventing the formation of R_{1-2}, the possibility for long-term disease control and/or cure is maintained. If the total population exceeds the threshold, adjust $\vec{d}(t)$ to minimize the predicted total population. We implement two threshold values in simulation studies: strategy 2.1:10^9 and strategy 2.2:10^{11}. Strategy 2 places prevention of the double-resistant mutant R_{1-2} at a higher priority than reduction of the total population, unless the total population has reached a threshold to threaten the patient's life. The rationale is that suppressing R_{1-2} maintains the chance of cure.

Strategy 3: Minimize the predicted total population unless there is a prediction that the first incurable cell will form within 45 days. Every 45 days, adjust $\vec{d}(t)$ to minimize the predicted total population if the predicted R_{1-2} population is <1. Otherwise adjust $\vec{d}(t)$ to minimize the predicted R_{1-2} population. The rationale is to switch to prevention of R_{1-2} only if the predicted risk of R_{1-2} emergence is prominent. However, if the current $x_{R12} \geq 1$ and R_{1-2} is not curable ($g_0 - S_a(R_{1-2},1) - S_a(R_{1-2},2) > 0$), minimize the predicted total population; that is, if R_{1-2} has already appeared, we no longer focus on preventing its appearance. Given that we allow for "relative" resistance, it is possible that R_{1-2} is not incurable; however, in most of our parameter settings, it is incurable.

Strategy 4: Estimate the time to either incurability or death, and react to the most proximal threat as long as there is a chance of cure. Every 45 days, evaluate the predicted durations toward incurability ($x_{R1-2} \geq 1$) and mortality (population $\geq 10^{13}$) dictated by the growth of S, R_1, R_2, and R_{1-2} populations. For each dosage combination $\vec{d}$, define $\tau_{inc}(\vec{d})$ as the predicted time to incurability ($x_{R1-2} \geq 1$), given the currently observed population and $\vec{d}$ fixed. Define $\tau_S(\vec{d})$ as the predicted time to x_S causing mortality ($x_S \geq 10^{13}$), given the currently observed population and $\vec{d}$ fixed. $\tau_{R1}, \tau_{R2}, \tau_{R1-2}$ can be defined in the same fashion. If the current $x_{R1-2} < 1$ or R_{1-2} is curable [i.e., there exists some $\vec{d}$ such that each component of $diag(S_a\vec{d}) > g_0$], vary $\vec{d}$ to maximize $\min(\tau_{inc}, \tau_S, \tau_{R1}, \tau_{R2}, \tau_{R1-2})$, with the constraint that $\min(\tau_S, \tau_{R1}, \tau_{R2}, \tau_{R1-2}) > 45$ days. If such a dosage combination does not exist, maximize $\min(\tau_S, \tau_{R1}, \tau_{R2}, \tau_{R1-2})$. If the current $x_{R1-2} \geq 1$ and R_{1-2} is not curable, maximize $\min(\tau_S, \tau_{R1}, \tau_{R2}, \tau_{R1-2})$. The rationale is to quantify the risk induced by each cell type as the predicted duration toward incurability or mortality and to find the dosage combination to minimize the risk.

Predicting Populations of Each Cell Type. Eq. **S1** can be solved analytically if $\vec{d}(t)$ is piecewise constant. This is the case for practical

treatments, because the dosages are altered only at fixed time intervals or when the current treatment regimen fails. Suppose with time interval $[0, T]$, $\vec{d}(t) \equiv \vec{d}$ is a constant. If all components of $\vec{x} > 1$, Eq. **S1** is then reduced to a first-order linear matrix differential equation:

$$\frac{d\vec{x}}{dt} = \left[(I + T)g_0 - diag\left(S_a\vec{d}\right)\right]\vec{x} \equiv A\vec{x}. \qquad \textbf{[S2]}$$

The solution of Eq. **S2** is simply the matrix exponential times of the initial population $e^{At}\vec{x}(0)$. This solution sustains as long as $\vec{d}(t)$ stays constant and all components of $\vec{x} > 1$.

If some components of $\vec{x} < 1$, (e.g., $x_{R1-2} < 1$), Eq. **S2** is no longer equivalent to Eq. **S1**. $U(\vec{x} - 1)\vec{x}$ sets fractional cell numbers to 0, and thus blocks their contribution to the growth rates. In this case, we define a matrix B such that the rows corresponding to the fractional populations are 0 and the remaining rows are equal to those of A. Hence, Eq. **S1** becomes

$$\frac{d\vec{x}}{dt} = B\vec{x}, \qquad \textbf{[S3]}$$

and the solution is $e^{Bt}\vec{x}(0)$. Eq. **S3** is valid only if the population of each cell type does not cross the boundary of one cell (increases from $x < 1$ to $x > 1$ and vice versa). When boundary crossing occurs, the constant matrix B has to be updated, and the population before boundary crossing is treated as the initial population for the new differential equation.

Prediction of each population is summarized as follows:

i) Divide time into regular intervals (45 days in this application), in which $\vec{d}(t)$ is constant within each interval but is allowed to vary between intervals.
ii) At the beginning of each interval, update Eq. **S1** by replacing $\vec{d}(t)$ with the new dosage combination and setting the initial population as the calculated population of the prior interval.
iii) Construct the constant matrix B from $[(I + T)g_0 - diag(S_a\vec{d})]$ $U(\vec{x} - 1) \equiv A$ and the initial population of the current interval. Set the rows of B corresponding to fractional populations to 0.
iv) Denote $\vec{x}(T_i)$ the initial population of the interval $[T_i, T_{i+1})$ and B_i the corresponding constant matrix in Eq. **S3.** The solution for $t \in [T_i, T_{i+1})$ is $\vec{x}(t) = e^{B_i(t-T_i)}\vec{x}(T_i)$ if entries of $\vec{x}(t)$ do not cross the single-cell boundary.
v) If boundary crossing occurs on $\tau \in [T_i, T_{i+1}]$, update B_i accordingly and set the initial population of Eq. **S3** to $\vec{x}(\tau)$.
vi) Continue matrix and initial population updates to the end of the total time considered (5 y in this study).

Simulation Studies. We carried out large-scale simulation studies to assess the effectiveness of each treatment strategy under different parameter settings. The following parameters in the cancer growth model and treatment strategies were varied in simulation experiments. The model parameter ranges were designed to bracket realistic parameter values based on clinical, in vitro, and in vivo data. By bracketing possible parameter values, we were able to state that the conclusions were robust and general across a broad range of individual tumors. All evaluable combinations of parameters over these broad ranges were investigated.

The initial total population was 5×10^9, roughly equivalent to a 5-cm^3 lesion.

The lookahead time of predicting responses under each fixed treatment strategy was 45 days, similar to the 6 wk that elapse between computed tomography (CT) evaluations on clinical studies.

Possible values for the ratio of the initial R_1 and total populations were 0, 10^{-9}, 10^{-7}, 10^{-5}, 10^{-3}, 0.1, and 0.9. Thus, the subpopulations vary from absent to only five cells; from four 2-log increments to 10%; and, finally, the case where they are the dominant population.

Possible values for the ratio of the initial R_2 and total populations were 0, 10^{-9}, 10^{-7}, 10^{-5}, 10^{-3}, 0.1, and 0.9. These values are the same as the ratio of the initial R_1 and total populations.

Possible values for a net growth rate (per day), g_0, were 0.001, 0.002642, 0.00698, 0.018439, 0.048714, 0.128696, and 0.34. The maximum value is a worst case scenario assuming a 48-h growth rate, 100% cells in cycle, and zero death rate (1–3). In contrast, the minimum value is a very slow-growing tumor that doubles in size over a 2-y period. The low range is roughly in accord with the range of growth rates that fit data from 228 patients with pancreatic cancer, 101 of whom also contributed autopsies (i.e., 0.005–0.02 per day) (4). The intermediate values represent equal log increments. A value of 0.055 corresponds to a relatively fast-growing realistic tumor that doubles in size in the 6-wk interval between CT scans.

The sensitivity of S to d_1 relative to the natural growth rate was $\frac{S_a(S,1)}{g_0}$. The ratio is < 1 if S is resistant to d_1. Possible values were 0.000560, 0.005379, 0.051674, 0.496387, 4.768310, 45.804544, and 440. A range of sensitivities was first derived. The minimum sensitivity of interest should be sufficient to cause a 25% increase in the progression-free survival (20% decrease in the instantaneous progression hazard) for the slowest growth rate tumor in the range listed above. That corresponds to the minimum effect size deemed of interest in clinical drug development programs. The maximum sensitivity was calculated to cause a 4-log decrease in cell count over 3 mo for the fastest growing tumor in the range listed above. The highest sensitivity to the growth rate ratio involved the highest sensitivity divided by the lowest growth rate. The lowest sensitivity to the growth rate ratio involved the lowest sensitivity divided by the highest growth rate. Between these extremes, the range was divided into equally spaced logarithmic intervals.

The sensitivity of S to d_2 over d_1 was $\frac{S_a(S,2)}{S_a(S,1)}$. Possible values were 0.000400, 0.001474, 0.005429, 0.020000, 0.073681, 0.271442, and 1. Here we assume that d_1 is more effective than d_2 against S cells. Because d_1 is superior to d_2 by convention, the highest possible value of this ratio is 1. The lowest possible value is the lowest sensitivity of interest divided by the highest sensitivity of interest. The range is divided into equally spaced logarithmic intervals.

The sensitivity of R_1 to d_1 over sensitivity of S to d_1 was $\frac{Sa(R_1,1)}{Sa(S,1)}$. Possible values were 0, 10^{-5}, 9.564×10^{-5}, 9.146×10^{-4}, 8.747×10^{-3}, 8.365×10^{-2}, and 0.8. These were picked arbitrarily to include 0 (complete resistance), 1×10^{-5} (considerable resistance), and 0.8 (minimal resistance), with equal logarithmic spacing of other values between 1×10^{-5} and 0.8.

The sensitivity of R_2 to d_2 over the sensitivity of S to d_2 was $\frac{Sa(R_2,2)}{Sa(S,2)}$. Possible values were 0, 10^{-5}, 9.564×10^{-5}, 9.146×10^{-4}, 8.747×10^{-3}, 8.365×10^{-2}, and 0.8. These values are identical to those immediately above.

The $S \rightarrow R_1$ transition rate (per cell division) was $T(R_1, S)$. Possible values were 10^{-11}, 2.154×10^{-10}, 4.642×10^{-9}, 10^{-7}, 2.154×10^{-6}, 4.642×10^{-5}, and 10^{-3}. Transitions can occur by any known genetic or epigenetic mechanism, including mutations, translocations, insertions, deletions, translocations, amplifications, copy number change, DNA methylation, and/or modification of histones. The total transition rate is the sum

of all possible transition rates over all relevant loci that alter the sensitivity/resistance phenotype. These loci may correspond to "driver" loci; however, in some cases, they correspond to "passenger" loci (i.e., some genetic changes, although not part of the original oncogenic mutations, may still drive resistance to therapy) (5). The lowest transition rate value assumes the WT mutation rate estimated for human stem cells (6). It is in accord with a minimal mutation burden in the most genetically stable tumor, yet sequenced, retinoblastoma (minimum 2.2×10^{-8} burden in a full tumor, or 2.2×10^{-10} or less per generation if 100 or more cell generations to generate the retinoblastoma are assumed) (7).

The highest transition rate value assumes this rate initially, a maximal mutator mutation of 50,000-fold increase in mutation rate (8), and many parallel pathways to acquire resistance (100 proteins, mutation of which could lead to resistance, each with 20 possible loci for mutation). Note that a typical protein is at least 100 amino acids, and, on average, 30% of loci inactivate enzymes when there is a nonsynonymous mutation (9). This rate is also ~10-fold the rate of genetic change per locus in cells with a chromosomal instability (CIN) mutation (10), allowing for 10 parallel pathways of resistance by CIN.

The range of 10^{-11} to 10^{-3} thus encompasses a broad range of possible values. It is in accord with modeling of data from a series of 228 patients with pancreatic cancer, 101 of whom had autopsies (4). The best fit to this data was with a genetic change rate of 6×10^{-5}, but all values within the range explored (10^{-9} to 10^{-4}) had nearly equally good fits.

The other values are at equally spaced logarithmic intervals.

Possible values for an $S \rightarrow R_2$ mutation rate (per cell division) $T(R_2, S)$ were 10^{-11}, 2.154×10^{-10}, 4.642×10^{-9}, 10^{-7}, 2.154×10^{-6}, 4.642×10^{-5}, and 10^{-3}. These values are identical to those directly above them.

There are $7^9 = 40,353,607$ total possible parameter configurations. For each configuration, we applied each of the six strategies (strategies 2.1 and 2.2 were treated as distinct strategies) independently. The population of each cell type was simulated every 45 days according to the imposed drug dosage and Eq. **S1**. The drug dosage for the following period was updated according to each of the six strategies. Simulation stopped if the total population of cancer cells exceeded 10^{13} or the simulation time exceeded 5 y. The survival period of each strategy in each parameter configuration was reported.

Due to the inclusion of extreme parameter values, the parameter combinations were then prescreened and the following combinations were eliminated from the final analysis: (*i*) any combination in which one of the two drugs was completely ineffective against all cell types, because there are no strategic choices in this case or (*ii*) any combination in which all treatment strategies resulted in survival greater than 4 y, corresponding to very slow growth rates or highly sensitive cells. Because the simulation was truncated at 5 y, and because a significant survival difference required at least a 25% improvement compared with a reference, it was not possible to ascertain if there was improvement if all strategies resulted in survival for longer than 4 y.

Comparison of Total Population Minimizing Strategy (Strategy 1) with Other Strategies Switching Between Minimizing Total and R_{1-2} Populations. Here, we compare strategy 1 with strategies 2.1, 2.2, 3, and 4. Strategy 1 minimizes the estimated total population and does not treat R_{1-2} differently. The other four strategies all have some scheme for switching between minimizing the total population and the R_{1-2} population.

At each time point, when deciding the drug dosage, we have to consider two types of risks: the risk from the R_{1-2} population and the risk from the remaining cell types. If strategy 1 is among the better strategies, then, in principle, the risk from the S, R_1, and R_2 populations should outweigh the risk from the R_{1-2} population. Thus, if we can quantify the risk from each population, we may predict whether strategy 1 works.

We quantify the risk from each population in the following way. Suppose we apply a single drug constantly to minimize a population and ignore the discrepancy of fractional counts, what is the time that it takes the target population to reach a mortal number? Formally, define

$$\begin{aligned} F_1 &= (I+T)diag(g_0) - diag(S_a\vec{d}_1) \\ F_2 &= (I+T)diag(g_0) - diag(S_a\vec{d}_2), \end{aligned} \quad \textbf{[S4]}$$

where $d_1 = [1,0]^t$ and $d_2 = [0,1]^t$. F_1 and F_2 are the growth rate matrices of applying d_1 or d_2 constantly.

For each population $i \in \{S, R_1, R_2, R_{12}\}$, define

$$\tau_i = \arg\min_t \left[\min\left((\exp(F_1 t)\vec{x}(0))_i, (\exp(F_2 t)\vec{x}(0))_i\right) \geq x_{mortal}\right]. \quad \textbf{[S5]}$$

τ_i is the estimated time that population i takes to reach the mortal threshold. We quantify the risks from each population with τ_i. A smaller τ_i implies a higher risk. The total risk of mortality, τ_{total}, can be estimated from the sum of the rates attributable to each τ_i:

$$\frac{1}{\tau_{total}} = \sum_i \left(\frac{1}{\tau_i}\right). \quad \textbf{[S6]}$$

In a similar manner, we define τ_{inc}, the time to incurability, as the estimated time until the first R_{1-2} cell forms, given that these cells are incurable:

$$\tau_{inc} = \arg\min_t \left[\min\left((\exp(F_1 t)\vec{x}(0))_4, (\exp(F_2 t)\vec{x}(0))_4\right) \geq 1\right], \quad \textbf{[S7]}$$

where x_4 is the number of the fourth cell type, R_{1-2}.

Conditions in which τ_{inc} is strictly minimum (i.e., $\tau_{inc} < \tau_{tot}$) should be more likely to have at least one of the strategies 2.1, 2.2, 3, and 4 superior to strategy 1. In fact, among virtual patients for whom this condition is met, strategy 1 is significantly inferior to either strategy 2.1, 2.2, 3, or 4 in 13.4% of cases, a 5.4-fold enrichment over when the condition is not met (Table S1).

Parameter Values for the Illustrative Case. In the illustrative case described in the main text, there is an initial undetected minority population of R_1 cells (preexisting undetected heterogeneity), rapid transition rates overall (rapid genetic dynamics), and a faster acquisition of R_2 resistance than of R_1 resistance (asymmetry).

The parameters are:

$$\frac{R_1}{N} = 10^{-5}$$

$$\frac{R_2}{N} = 0$$

$$\frac{R_{1-2}}{N} = 0$$

$$g_0 = 0.05 \text{ (all cell types)}$$

$$S_a(S,1) = 0.15$$

$$S_a(R_1, 1) = 0.0225$$

$$S_a(R_1, 2) = 0.15$$

$$S_a(R_2, 1) = 0.15$$

$$S_a(R_2, 2) = 0.0225$$

$$S_a(R_{1-2}, 1) = 0.0225$$

$$S_a(R_{1-2}, 2) = 0.0225$$

Transition rate to resistance to $d_1 : 4 \times 10^{-9}$
Transition rate to resistance to $d_2 : 4 \times 10^{-7}$

Linkage of Core Model to Other Models. The current model focuses on drug sensitivity/resistance phenotypes as determined by genetic and epigenetic factors and their influence on optimal personalized medicine factors. The focus on heritable phenotypes and the condensation of a very large number of genotypes onto a smaller number of phenotypic clusters are both essential to allow computationally feasible evaluation of complex treatment strategies. We term this focused model the "core model." Supported by extensive sensitivity analysis over a broad range of parameters, the core model has produced high-level conclusions about personalized medicine strategies.

In applying this core model in detail to real tumors, many additional complexities will need to be taken into account. These additional complexities will need to be evaluated by separate linked models, which then feed information to the core model. This framework of linked models then allows representation of the complexities of individual tumors and therapies so that detailed conclusions can be drawn. This is a more efficient approach for a complex system in that properties of individual tumors can be computed in separate steps and then applied to a large number of candidate treatment strategies.

When applied to real tumors, the core model will, in many cases, need to specify probability distributions of parameter values rather than discrete values. The current core model uses broad ranges of parameter values with a uniform distribution (each value of the parameter is assigned equal probability); however, when linked to other sources of information, these probability distributions may be narrowed down and become more structured. Below, we give a high-level concept of how the core model would assimilate information from other models about (*i*) the heritable states underlying a sensitivity or resistance phenotype and transitions between these states, (*ii*) passenger vs. driver mutations, (*iii*) nongenetic mechanisms of resistance, and (*iv*) biodistribution.

Sources of information for mapping phenotypic states onto genetic states and for estimation of transition rates. The following sources would be used to get a mapping between phenotypic sensitivity/resistance states and underlying genotypes, as well as to estimate the probability of existence of a particular state:

i) Direct measurement: This requires the development of noninvasive methods for sampling and molecular and/or phenotypic characterization at the single-cell level.

ii) Empirical databases: By collecting information on a large number of patients at diagnosis and autopsy, one can begin to characterize the possible states and their likelihood of occurrence empirically. For example, in a recent paper (11), the detailed subclonal structure of ~100 triple-negative breast cancers was presented, albeit not yet at single-cell resolution. Molecular studies of panels of cell lines can be used to supplement this empirical information, and these cell lines can be directly tested for drug sensitivity phenotypes to correlate with the genetic and epigenetic annotations (12).

iii) Computational pathway analysis: As an example PARADIGM software (University of California at Santa Cruz Cancer Genomics Browser) can analyze over 1,400 curated signaling pathways. Such software may be used in the future in an attempt to predict what molecular substates may be associated with a particular sensitivity profile in that a variety of specific modifications might present with similar phenotypic effects analyzed at the pathway level (13). By using this software, it might be possible to predict additional genetic states associated with a phenotype based on their pathway relationship to others that had been determined experimentally.

iv) Functional genomics: High-throughput screens with siRNA and shRNA can be applied systematically to predict what genotypes might be associated with sensitivity and resistance phenotypes (14).

The transitions between these states may be by any mechanism, not limited to mutations of a single driver gene but including all known mechanisms of genetic and epigenetic change (mutation, insertion, deletion, translocation, amplification, chromosome loss or gain, DNA methylation, or histone modification). The total transition rate between phenotypic states A and B is the sum of the rates corresponding to all possible ways of getting from phenotype A to phenotype B. Given that we may not know which of many underlying molecular states is currently resulting in phenotype A, we may have to calculate the rate of transition to B for each possible molecular state underlying phenotype A and add up all these rates, each multiplied by the probability of a particular molecular state underlying the phenotype. For any individual rate, we will need to know how similar the two molecular states are and the rates of possible interconversion mechanisms. Because genetic instability mutations may affect these individual rates, the individual rates themselves may need to be represented as ranges or probability distributions.

Driver and passenger mutations. The model is fundamentally a model of phenotypic transitions between drug sensitivity states, and the phenotypic transition may occur via any of a large number of possible genetic changes. The total rate of phenotypic change is the sum of the rates from all the individual changes that could, in principle, lead to the phenotypic change. For drug resistance, this could be by acquisition of a new driver mutation that circumvents the previous therapy, but it could also be due to a passenger mutation. Such a mutation, although not implicated in driving the tumor originally, may drive resistance. For example, a mutation may occur that leads to alterations in cellular distribution or metabolism of the drug. We have previously written about the fact that passenger mutations represent a reservoir of diversity that may also contribute to drug resistance, and therefore survival under drug therapy (5).

Passenger mutations differ from driver mutations in that they are not selected for in the absence of therapy. This is reflected in the net growth rate parameters in the absence of drug therapy in the model, which will not reflect an increase in growth rate with the acquisition of a passenger mutation.

Nongenetic changes. Known mechanisms of resistance to vemurafenib also exemplify resistance mechanisms that do not involve genetic change (15, 16). In particular, in colorectal cancer, vemurafenib inhibition of B-Raf leads to feedback up-regulation of EGF receptor (EGFR), in turn, leading to two events: (*i*) upstream activation of Ras, leading to dimerization of B-Raf, rendering vemurafenib ineffective and (*ii*) parallel activation of the pI3-kinase signaling pathway, potentially circumventing the Ras-Raf-Mek pathway to the extent that it may still be inhibited. This resistance is hard-wired, occurs rapidly, and does not re-

quire genetic change. Such feedback loops are common in signaling pathways, and, in fact, a similar feedback loop affects pI3-kinase pathway inhibitors (17).

In the main text, we state that "'drug-1' and 'drug-2' may also refer to combinations directed at single states." This statement has a very specific meaning: in a case such as vemurafenib in colorectal cancer, vemurafenib clearly should be given in combination with an EGFR inhibitor. If the heritable state is that described for colorectal cancer (15), drug-1 means an optimized drug or drug combination for the transient adaptations that can be assumed within that heritable state (i.e., a combination, such as vemurafenib and cetuximab). The optimized combination must be determined by a linked model separate from the core model. High-content phosphoproteomics (18) is an important source of information in attempting to understand signaling as it relates to nongenetic mechanisms of resistance.

In some cases, an optimized combination to deal with nongenetic resistance is not available. In this case, that fact is reflected in lesser net efficacy parameter input into the model. In other cases, nongenetic resistance may be variable. In this case, it can be represented by a probability distribution of the efficacy parameter. This probability distribution could be different in different genetic states; that is, genetic states could influence the likelihood of a particular resistance mechanism. All this can be input into the parameter distributions in the model if it is known.

Biodistribution. Just as drug-1 and drug-2 are optimized combinations if necessary to deal with nongenetic resistance mechanisms, the dose and schedule of drug-1 or drug-2 given as a single agent are assumed to be optimized with respect to drug delivery. To the extent that the continuum of intratumoral concentrations corresponding to a dose is known, this information can be fed into the core model's efficacy parameter distribution. We are actively researching the problem of determining the optimal dose for antibodies as a function of their biodistribution (19) and the biophysical factors that determine this (20). These problems are largely unsolved, but information can be fed from complex models of this phenomenon into the core model if available.

1. Baca OG, Scott TO, Akporiaye ET, DeBlassie R, Crissman HA (1985) Cell cycle distribution patterns and generation times of L929 fibroblast cells persistently infected with Coxiella burnetii. *Infect Immun* 47:366–369.
2. Baker FL, Sanger LJ, Rodgers RW, Jabboury K, Mangini OR (1995) Cell proliferation kinetics of normal and tumour tissue in vitro: Quiescent reproductive cells and the cycling reproductive fraction. *Cell Prolif* 28(1):1–15.
3. MITOPENCOURSEWARE (2005) Cell, tissue and tumor kinetics. Available at http://ocw.mit.edu, accessed January 6, 2005.
4. Haeno H, et al. (2012) Computational modeling of pancreatic cancer reveals kinetics of metastasis suggesting optimum treatment strategies. *Cell* 148:362–375.
5. Beckman RA (2010) Efficiency of carcinogenesis: Is the mutator phenotype inevitable? *Semin Cancer Biol* 20:340–352.
6. Cervantes RB, Stringer JR, Shao C, Tischfield JA, Stambrook PJ (2002) Embryonic stem cells and somatic cells differ in mutation frequency and type. *Proc Natl Acad Sci USA* 99:3586–3590.
7. Zhang J, et al. (2012) A novel retinoblastoma therapy from genomic and epigenetic analyses. *Nature* 481:329–334.
8. Camps M, Naukkarinen J, Johnson BP, Loeb LA (2003) Targeted gene evolution in *Escherichia coli* using a highly error-prone DNA polymerase I. *Proc Natl Acad Sci USA* 100:9727–9732.
9. Guo HH, Choe J, Loeb LA (2004) Protein tolerance to random amino acid change. *Proc Natl Acad Sci USA* 101:9205–9210.
10. Lengauer C, Kinzler KW, Vogelstein B (1997) Genetic instability in colorectal cancers. *Nature* 386:623–627.
11. Shah SP, et al. (2012) The clonal and mutational evolution spectrum of primary triple-negative breast cancers. *Nature* 486:395–399.
12. Barretina J, et al. (2012) The Cancer Cell Line Encyclopedia enables predictive modelling of anticancer drug sensitivity. *Nature* 483:603–607.
13. Heiser LM, et al. (2012) Subtype and pathway specific responses to anticancer compounds in breast cancer. *Proc Natl Acad Sci USA* 109:2724–2729.
14. Jiang H, Pritchard JR, Williams RT, Lauffenburger DA, Hemann MT (2011) A mammalian functional-genetic approach to characterizing cancer therapeutics. *Nat Chem Biol* 7(2):92–100.
15. Prahallad A, et al. (2012) Unresponsiveness of colon cancer to BRAF(V600E) inhibition through feedback activation of EGFR. *Nature* 483:100–103.
16. Solit DB, Jänne PA (2012) Translational medicine: Primed for resistance. *Nature* 483 (7387):44–45.
17. Chandarlapaty S, et al. (2011) AKT inhibition relieves feedback suppression of receptor tyrosine kinase expression and activity. *Cancer Cell* 19(1):58–71.
18. Anderson JN, et al. (2010) Pathway-based identification of biomarkers for targeted therapeutics: personalized oncology with PI3K pathway inhibitors. *Sci Transl Med* 2: 43–56.
19. Beckman RA, von Roemeling R, Scott AM (2011) Monoclonal antibody dose determination and biodistribution into solid tumors. *Therapeutic Delivery* 2: 333–344.
20. Beckman RA, Weiner LM, Davis HM (2007) Antibody constructs in cancer therapy: Protein engineering strategies to improve exposure in solid tumors. *Cancer* 109(2): 170–179.

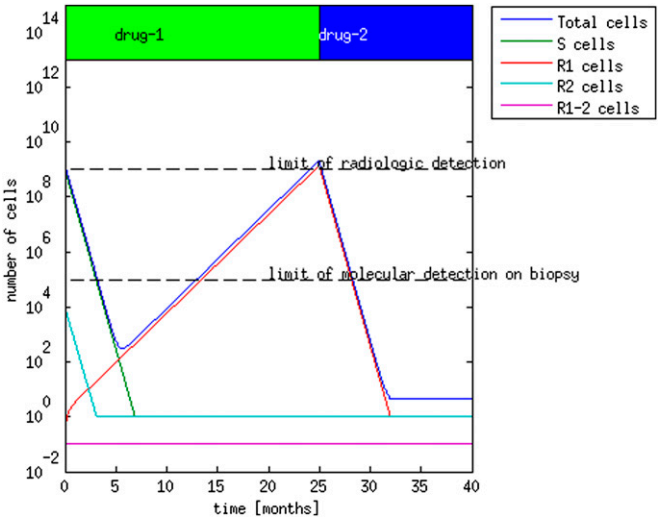

Fig. S1. Supplementary illustrative case treated by the current personalized medicine strategy. Time (months) is on the *x* axis, and cell number is on the *y* axis. The total number of cells (*N*) is shown in blue (multiplied by 1.5 to create separation from the predominant population for clarity), *S* cells are shown in green, R_1 cells are shown in red, R_2 cells are shown in light blue, and R_{1-2} cells are shown in magenta. Treatments are indicated by the solid bars at the top: green is drug-1, blue is drug-2, and both colors indicate a combination. The patient is treated with drug-1 and experiences a complete response, only to relapse 25 mo after diagnosis with R_1 cells. He/she is then treated with drug-2, experiencing a cure 32 mo after initial diagnosis.

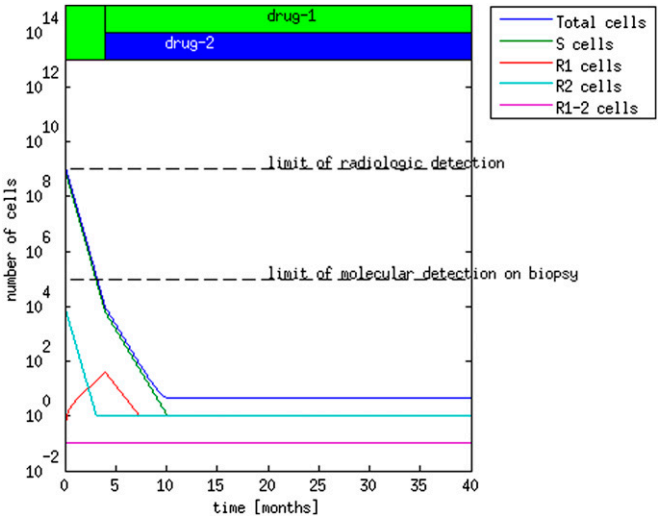

Fig. S2. Supplementary illustrative case treated by the nonstandard personalized medicine strategy. Time (months) is on the *x* axis, and cell number is on the *y* axis. The total number of cells (*N*) is shown in blue (multiplied by 1.5 to create separation from the predominant population for clarity), *S* cells are shown in green, R_1 cells are shown in red, R_2 cells are shown in light blue, and R_{1-2} cells are shown in magenta. Treatments are indicated by the solid bars at the top: green is drug-1, blue is drug-2, and both colors indicate a combination. The patient is treated with drug-1 for 4 mo and then with an equal combination of drug-1 and drug-2, experiencing a rapid cure in 10 mo.

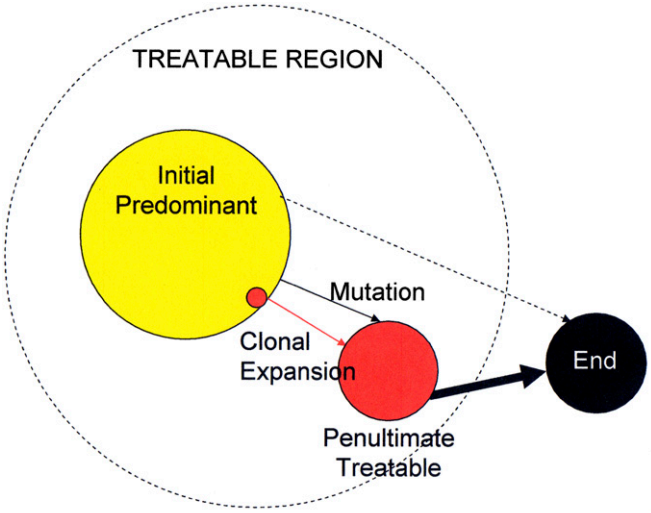

Fig. S3. Graphical representation of phenotypic states in genetic space, illustrating a nonstandard personalized medicine scenario. The large dashed circle represents the genetic space that is treatable by available therapies. The three solid circles represent genetic states that can correspond to phenotypic states. The large yellow circle is the predominant state of the majority of cells at initial diagnosis ("initial-predominant state"). The black circle, outside the treatable space, is a lethal incurable state ("end state"). The small red circle within the treatable space is a "penultimate treatable state." It is treatable because it is still within the dashed circle, but it is a penultimate treatable state in that it is genetically close to the end state. Its smaller size indicates that at initial diagnosis, it had fewer cells and perhaps was even undetectable. The threat from the initial-predominant state is significant (yellow) because it contains the largest tumor burden. However, the threat from the penultimate-treatable state is greater (red) because of its proximity to the end state. Black arrows represent genetic transitions, the dashed black arrow indicates that several steps are required, and solid arrows represent single-step transitions. The thick arrow denotes a faster transition, either because there are multiple parallel genetic pathways to the phenotype or because the starting state has a mutator phenotype. The penultimate-treatable state may be preexisting at diagnosis (small red circle inside initial-predominant state) and undergo clonal expansion (red arrow), or it may arise from the initial predominant state by mutation (black arrow).

Table S1. Conditions under which strategy 1 is significantly inferior

	No. of cases strategy 1 significantly worse* than strategy 2, 3, or 4	No. of cases strategy 1 not significantly worse* than strategy 2, 3, or 4
τ_{1-2} strictly minimum	36,670	236,056
τ_{1-2} not strictly minimum	4,532	176,188

*A strategy is defined as significantly better than another if it provides at least 8 wk of absolute and 25% relative improvement in overall survival.

Table S2. Comparison of current personalized medicine strategy and nonstandard personalized medicine strategy

	Current personalized medicine strategy	Nonstandard personalized medicine strategy
Molecular characteristics	Focus on average or consensus characteristics	Minority characteristics may be important
Disease course	Focuses on initial or current states	Focuses on end game, especially penultimate treatable states*
Strategy horizon	Current and (sometimes) next maneuver	Attempts to think several steps ahead
Mathematical optimization	May contribute to predictive markers for current step	Global or piecewise optimization over treatment course

*Penultimate treatable states are defined in the legend for Fig. S3.